Available online at www.sciencedirect.com

ScienceDirect

Advances in Space Research 67 (2021) 834–844

ADVANCES IN SPACE RESEARCH (a COSPAR publication)

www.elsevier.com/locate/asr

Compatibility of Terrestrial Reference Frames used in GNSS broadcast messages during an 8 week period of 2019

Stephen Malys [a,*], Russell Solomon [b], Jason Drotar [b], Todd Kawakami [a], Thomas Johnson [a]

[a] National Geospatial-Intelligence Agency, Research Directorate 7500 GEOINT Drive, Springfield, VA 22150-7500, USA
[b] Naval Surface Warfare Center 17214 Avenue B, Suite 128, Dahlgren, VA 22448, USA

Received 28 July 2020; received in revised form 9 November 2020; accepted 26 November 2020
Available online 5 December 2020

Abstract

The operational Terrestrial Reference Frames (TRFs) realized through the evaluation of broadcast ephemerides for GPS, GLONASS, Galileo, BeiDou-2 and BeiDou-3 have been compared to IGS14, the TRF realized by the International GNSS Service (IGS). The TRFs realized by the GPS, GLONASS, Galileo, and BeiDou-2 and BeiDou-3 broadcast ephemerides are the orbital realizations of WGS 84 (G1762′), PZ90.11, GTRF19v01, and BDCS respectively. These TRFs are compared using up to 56 days of data (21 July-14 Sept 2019) at a 5 or 15-min rate. The operational TRFs are compared to IGS14 in a 7-parameter similarity (Helmert) transformation. Numerical results show that the operational GNSS TRFs differ from IGS14 at a level no greater than 4 cm for Galileo, 6 cm for GPS and BeiDou-3, 13 cm for GLONASS, and 48 cm for a limited set of BeiDou-2 Medium Earth Orbit (MEO) vehicles.

Keywords: GNSS; Terrestrial Reference Frames; Broadcast Ephemerides

1. Introduction

A longtime goal in the discipline of geodesy has been the establishment of an accessible, common global Terrestrial Reference Frame (TRF) usable for all types of geospatial information on or near the surface of the Earth. This ideal TRF would have its origin at the center of mass of the Earth, its 3 orthogonal Cartesian axes fixed to the rotating Earth with no net rotation due to plate tectonics and a scale that conforms to universally adopted length units established in the System International (SI) conventions.

The invention of satellite navigation at Johns Hopkins University/Applied Physics Laboratory in the 1950s and the success of the United States' NAVSTAR Global Positioning System (GPS) have, in part, motivated Russia, China, and the European Union to develop their own versions of a Global Navigation Satellite System (GNSS), which, out of necessity, have achieved their own realizations of a TRF. All of these GNSS developments have allowed mapping organizations around the world to slowly begin phasing out the use of classical horizontal mapping datums such as the European Datum 1950, Tokyo Datum, North American Datum 1927, Pulkova 1942, and the hundreds of other classical horizontal mapping datums developed over several centuries.

The International science community, represented in the International GNSS Service (IGS) (Dow et al., 2009), International Laser Ranging Service (ILRS) (Pearlman et al., 2002), International VLBI Service (IVS) (Schuh and Behrend, 2012), International DORIS Service(IDS), (Willis et al., 2010), and International Earth Rotation and Reference Systems Service (IERS) (Dick and Thaller, 2018) has steadily advanced the state of the art TRF by

* Corresponding author.
E-mail addresses: stephen.malys@nga.mil (S. Malys), jason.drotar@navy.mil (J. Drotar), todd.kawakami@us.af.mil (T. Kawakami), thomas.j.johnson@nga.mil (T. Johnson).

https://doi.org/10.1016/j.asr.2020.11.029
0273-1177/Published by Elsevier Ltd on behalf of COSPAR.

contributing to the development of a series of International Terrestrial Reference Frames, the latest being named ITRF2014 (Altamimi et al., 2016, 2017).

With all of these science community improvements in the past few decades, there is an important TRF question for real-time GNSS users, navigators, and mapping organizations dependent on individual or multiple GNSS: How compatible or how coincident are the various TRFs realized through each GNSS? Note that the vast majority of GNSS users are not in the science community and therefore not directly using ITRF2014 as their TRF. Rather, they are using GNSS for countless everyday practical applications. Also, note that the methodology and results reported here are only valid for direct, real-time unaugmented GNSS applications. Any form of augmentation including all types of differential positioning, Assisted GPS, or specialized augmentation, such as the US Federal Aviation Administration (FAA's) Wide Area Augmentation System, immediately introduce an alternate TRF with its own relationship to ITRF2014.

Similar to the TRF compatibility we report on here, the GNSS time offsets are an important issue for a multi-GNSS user. Like the TRFs, each GNSS realizes its own overall system time and the differences among these time scales must be assessed, quantified and addressed. While we do not examine that issue here, we refer readers to Lewandowski et al. (2011) for a description and overview of the fundamental concepts influencing GNSS time scales and Nicolini and Caporali (2018) for analysis and numerical results from more than 3 years of data assessing time scale biases and 1 week of data assessing TRF biases.

Since TRFs used in all GNSS operations as well as those developed and used by the scientific community are subject to on-going incremental periodic or aperiodic improvements, we note the importance of clearly identifying the date(s) of the assessment(s) and the length of the data period studied. Our work presented here for example, as indicated by the title of the paper, is from an 8 week period in 2019. A number of earlier studies using specific, more limited periods of GNSS data from single or multiple GNSS constellations or ground networks where a TRF was assessed are available. A few examples of earlier TRF compatibility studies are Malys et al. (1984), Boucher and Altamimi (2001) and Nicolini and Caporali (2018). In all cases involving the current set of GNSS, the prevailing ITRF, here in the form of its GNSS realization: IGS14 for example, has been used as the best available realization of a global TRF. The TRF used as a 'truth standard' is realized by either a network of monitor stations on the Earth's crust or a set of satellite ephemerides estimated by the IGS.

To promote interoperability and international cooperation, the United Nations Office for Outer Space Affairs (UNOOSA) coordinates the International Committee on GNSS (ICG). Within this ICG a specific Working Group (D) exists where annual presentations are made by each GNSS 'provider' on the status of their operational TRF. Under this Working Group, Enderle (2018) provides one example where the operational Galileo TRF is presented and compared to ITRF2014 (specifically the IGS14 realization). In this same Working Group, Liu et al. (2018) presented the status of the BeiDou operational TRF. Moreover, other efforts performed under this Working Group such as Petit and Delporte (2019) focus on the questions of interoperability among GNSS time scales.

To our knowledge, the study presented here uses the largest data set analyzed to date for operational TRF compatibility among the 4 globally-available GNSSs.

2. Methodology and data sets

This study attempts to answer the above question by comparing the operational Terrestrial Reference Frames realized through broadcast navigation messages to the science community's TRF realized through the post-fit Multi-GNSS Experiment (MGEX) (Montenbruck et al., 2017). This post-fit MGEX TRF is known as IGS14 (Rebischung et al., 2016a; Griffiths, 2019), mentioned above and representing the IGS (Dow et al. 2009, Johnston et al. 2017) GNSS realization of the International Terrestrial Reference Frame 2014 (ITRF, 2014) (Altamimi et al., 2016, 2017).

Recall that all broadcast GNSS ephemerides are predictions that must be used for direct (non-augmented) real-time Positioning, Navigation and Timing (PNT). These broadcast ephemerides certainly contain a level of prediction error but also facilitate a real-time realization of the operational Earth-Centered, Earth-Fixed Terrestrial Reference Frame, accessible to an unlimited number of users. These orbital realizations of a TRF are based of course on the ground-based realizations of each system provider's operational TRF – the known positions and velocities of the network of monitor station antennas employed in the operation of each GNSS. Each operational orbit-based TRF is accessible by following procedures documented in respective space to user segment Interface Control Documents (ICDs) of each GNSS. Those procedures are documented in NAVSTAR (2020), RISDE (2008), EU (2016) and CNSO (2016) respectively. All GNSS receiver manufacturers use these procedures to perform real-time navigation, positioning and timing functions.

Ideally, TRFs are best compared in a 7-parameter or 14-parameter (including rates of change) set of transformation parameters using coordinates of stationary ground-based monitor stations employed in the operational GNSS ground segments. Since we do not have access to such coordinates for the four global GNSS in the TRFs under study, our next best choice is to compare the coordinates of corresponding satellite position vectors. These satellite position vectors obtained from broadcast messages are the orbital realizations of a TRF that billions of real-time GNSS users have access to.

The best publicly available ephemerides for GPS, GLONASS, Galileo, BeiDou-2 and BeiDou-3 are generated by

the organizations participating in the Multi-GNSS experiment (MGEX). MGEX is an effort coordinated by the International GNSS Service (IGS) and based on a TRF known as IGS14, the IGS' GNSS realization of the ITRF 2014. IGS14 was implemented in IGS processing on 29 Jan 2017 (Rebischung et al., 2016b) and maintained until 16 May 2020 (IGS Mail 7921).

Note that MGEX is the extension of a project known as the International GLONASS Service Pilot Project (IGLOS). This project was officially started in February 2000 and ended in 2005 when GLONASS data and products had been successfully integrated into the standard operations of the IGS. Its goals and objectives were similar to the International GLONASS Experiment (IGEX-98) (Willis et al, 1999; Slater et al., 1999). As such, the work and results presented here represent a Multi-GNSS version and contribution to addressing several of the goals outlined in these projects from more than 20 years ago. At that time, GPS and GLONASS were the only GNSS operating. Clearly, many investments, advancements and improvements have occurred since that time in the operational GNSS 'provider' community as well as the GNSS scientific community. The study presented here represents a convergence of these two communities on the specific topic of TRFs.

Using data sets covering a period of up to 56 Days (21 July-14 Sept, 2019, corresponding to GPS weeks 2063–2070), the Terrestrial Reference Frames used in broadcast ephemerides during that period were:

GPS WGS 84 (G1762′) (Malys et al., 2016)

GLONASS PZ-90.11 (Gusev, 2019)

Galileo GTRF19v01 (Enderle, Personal Communication, November 2019)

BeiDou BDCS(2019v01) (Liu et al., 2019).

Note that the TRF designated as 'WGS 84 (1762′)' differs slightly from 'WGS84 (G1762)' (without the prime) because 7 NGA monitor station antennas were individually replaced or re-located after GPS week 1762 (the week beginning 13 Oct 2013). For practical operational reasons, at various dates between Aug 2014 and June 2015, NGA analysts re-estimated individual station coordinates and velocities for each of these stations in the global G1762 TRF. For this reason, the 'prime' after the GPS week number (G1762′) simply indicates this TRF is an updated TRF realization, based on the full network solution (G1762). This WGS 84 (G1762′) TRF has been implemented, with any minor updates due to individual antenna changes, at 2SOPS, on an annual update cycle beginning with January 2016. The designation G1762′ has remained in effect throughout the 2019 data period studied here. As mentioned above, the broadcast navigation messages represent the orbital realization of the TRF established by the monitor station network.

Except for BeiDou-3, the corresponding MGEX ephemerides in IGS14 used for this study are those generated by the German organization GFZ (Deutsches GeoForschungsZentrum), Potsdam. These ephemerides are provided at a 5-minute rate. For BeiDou-3, ephemerides from Wuhan University were used. These ephemerides are provided at a 15-minute rate and some gaps exist in the coverage of the time span considered in this study; files for days 206, 222, 228, 232–234, and 239 were missing. All broadcast and MGEX ephemerides were obtained from the NASA Crustal Dynamics Data Information System (Noll, 2010) via ftp://cddis.gsfc.nasa.gov/pub/gps/products/mgex. The expected maximum number of data points available during the study period can be computed using the fact that there are 288 5-minute epochs in 24 h and multiplying that value by the number of days used in the analysis (56, except for BeiDou-3) and further multiplying by the number of healthy satellites available in each GNSS. For the 15-minute Wuhan files, there are 96 15-minute epochs in 24 h and 49 days of data (due to the 7 missing days). These upper limits along with the actual percentage of points used are shown in Table 1. Also shown are the satellites used and the number of stations used to obtain the navigation messages. A voting algorithm was used to select the navigation message, for a given satellite at a given time. The selected message was based on votes that were tabulated by the most stations, considering all fields except for transmission time (or message frame time, for GLONASS). The transmission time (or message frame time, for GLONASS) for a given message was taken to be the earliest time reported for any message considered equivalent to the message with the most votes. For GPS, LNAV messages were used while for Galileo, only messages with bits 1 and 8 set in the data sources field (corresponding to F/NAV E5a-I and E5a/E1 clock parameters) were used. In all cases, a large number of IGS stations, as shown in Table 1, were used in the broadcast message voting algorithm.

For a given navigation message, the satellite's orbit position and clock offset were computed, for a given time, as described in the interface control document (ICD) for the respective constellation. Furthermore, a given navigation message was only used for times at or later than the transmission time (or message frame time, for GLONASS) and within two hours of the message's epoch (or within 15 min of the epoch, for GLONASS). This process replicates how a real-time GNSS user would use the broadcast messages. The navigation messages yield Earth-centered, Earth-fixed (ECEF) positions for the antenna phase center (APC), while the MGEX ephemerides consist of ECEF positions for the center of mass. To allow comparison of positions, the navigation message positions should be moved to the center of mass using the same yaw model and antenna offsets that were used in generating the navigation message. While the exact yaw model used is not known in most cases, it is known that most of the satellites maintain close to nominal attitude. The GPS IIR satellites were assumed to maintain nominal attitude exactly, while the GPS IIF satellites were assumed to behave in the manner described by Dilssner (2010). A more accurate yaw

Table 1
Satellites, tracking networks, and numbers of data points used for each constellation.

Constellation	# of Satellites	# of IGS Stations Used to Obtain Navigation Messages	Satellites Tracked (SVN)	Max possible points	% of Max possible points used
GPS	31	140	34, 41, 43–48, 50–53, 55–73	499,698	99.2
GLONASS	21	128	716, 717, 719–721, 723, 730–732, 735, 736, 742–745, 747, 802, 851, 853–855	338,688	94.0
Galileo	22	132	101–103, 203, 205–222	354,816	99.4
BeiDou-2	5 GEO	49	3, 6, 11, 16, 18	80,640	94.3
BeiDou-2	7 IGSO	73	5, 7–10, 17, 19	112,896	99.1
BeiDou-2	3 MEO	96	12, 13, 15	48,384	96.7
BeiDou-3	18 MEO	96	201–216, 218, 219	84,672	75.3

model for the IIR satellites was considered unnecessary, given that the antenna offsets are nearly zero in the x/y-plane and that deviations from nominal do not last for very long. The GPS IIA satellite (SVN 34) was modeled using the yaw model described by Bar-Sever et al. (1996) with a maximum yaw rate of 0.123°/s and a yaw bias of 0.5°. For Galileo, the satellites were assumed to maintain nominal attitude except when doing so would exceed a maximum yaw rate of 0.06°/s, in which case the noon or midnight turn was performed at the maximum yaw rate and was symmetric about noon or midnight. For GLONASS, the yaw model described by Dilssner et al. (2010) for GLONASS-M satellites was used for all GLONASS satellites, with a maximum yaw rate of 0.25°/s. The BeiDou GEO satellites were assumed to be in an orbit-normal mode, as described by Montenbruck (2015), in which the + x axis points in the along-track direction. Except for certain satellites (noted below), the BeiDou-2 MEO and IGSO satellites were assumed to maintain nominal attitude, except when the sun elevation angle was below 4°, in which case orbit-normal mode was maintained. The transition between modes was assumed to occur at orbit dawn. Dilssner (2017, 2018) noted that some BeiDou-2 satellites do not actually go into orbit-normal mode. Based on his recommendations, the BeiDou-2 IGSO satellites with SVNs 5, 17, and 19 were assumed to not go into orbit-normal mode, and a maximum yaw rate of 0.085°/s was used, with symmetric noon and midnight turns. The BeiDou-2 MEO satellite with SVN 15 was also assumed to not go into orbit-normal mode, and a maximum yaw rate of 0.159°/s was used, with symmetric noon and midnight turns. This is the same assumption that was used for the BeiDou-3 MEO satellites, since it is believed that none of the BeiDou-3 MEO satellites use orbit-normal mode.

In addition to the yaw model, the antenna phase center offsets used by the system providers must be known in order to move the navigation message positions to the satellite's center of mass. In Table 2, GPS satellite antenna offset values published by NGA and used by the GPS ground segment (2nd Space Operations Squadron, 2SOPS) are shown. For comparison, the corresponding values provided in the IGS ANTEX file (Schmid et al., 2016; IGS ANTEX File, Week 2091), are also shown. The large discrepancy between the NGA and IGS ANTEX offsets underscores the importance of having the correct system provider offsets, given the very large differences that can exist between one source and another. While the values used by NGA have been published in the past (NGA, 2018), the GPS satellite antenna offsets used by 2SOPS have, for the first time, been approved for public release by the US Space Force as part of this publication (Kovach, Personal Communication, April 2020). For consistency purposes within the Department of Defense, the values used by NGA and those used by 2SOPS have been identical since 1989 when NGA began producing 'precise' GPS ephemerides and clock states. The NGA/2SOPS values are used in this study. For Galileo, since we are using E5a/E1 based navigation messages, we used the ionosphere-free combination of the E1 and E5a offsets from the IGS ANTEX file. It is noted that the offsets in the IGS ANTEX file are nearly identical to those from the Galileo metadata page (EU, 2020). Since the BeiDou navigation message is referenced to B3 (Montenbruck and Steigenberger, 2013) the B3 antenna phase center offsets from the BeiDou ANTEX file (CNSO, 2020) were used. For GLONASS, the values provided by Montenbruck (2015) for L1/L2 were used.

3. Data editing and parameter estimation

A data point for a given satellite at a given time was excluded if the satellite was set unhealthy, experiencing a clock event or orbit maneuver (as indicated by the corresponding flag in the MGEX SP3 file), or had unusable or absent clock data (as indicated by a clock offset of 999999.999999 in the MGEX SP3 file). Also, a point was excluded if the globally-averaged Signal in Space Range Error (SISRE) exceeded a designated threshold of 100 m. The SISRE we utilize is as defined by equation (45) and Table 4 of Montenbruck (2018). This SISRE is computed from the difference between a broadcast ephemeris point and the corresponding MGEX ephemeris point. While we are not using the satellite clock states in our process to estimate the 7 TRF parameters we seek, these states contribute to the SISRE and we further use these clock states as an

Table 2
GPS satellite antenna offsets (with respect to the center-of-mass) in use during the data period studied.

	NGA and 2SOPS Values			IGS ANTEX Values*			
GPS SV	Δx (cm)	Δy (cm)	Δz (cm)	Δx ' (cm)	Δy ' (cm)	Δz ' (cm)	Difference in z (cm)
Blk IIA PRN18/SVN34	27.9	0.0	95.2	27.9	0.0	235.2	140.1
Blk IIR PRN02/SVN61	1.0	−0.6	−8.2	0.1	−0.1	72.9	81.1
Blk IIR PRN11/SVN46	−0.2	−0.1	151.4	−0.1	−0.1	111.8	−39.6
Blk IIR PRN13/SVN43	−0.2	−0.3	161.4	−0.2	−0.2	134.8	−26.6
Blk IIR PRN14/SVN41	−0.2	0.0	161.4	−0.3	−0.2	130.4	−30.9
Blk IIR PRN16/SVN56	1.0	−0.6	166.3	1.3	−0.7	146.9	−19.4
Blk IIR PRN19/SVN59	0.8	−0.5	−1.8	0.9	−0.1	80.8	82.6
Blk IIR PRN20/SVN51	−0.2	−0.1	161.4	0.1	−0.3	131.4	−30.0
Blk IIR PRN21/SVN45	−0.2	0.1	158.4	−0.3	0.3	135.9	–22.5
Blk IIR PRN22/SVN47	−0.2	0.1	6.0	−0.2	0.2	85.1	79.1
Blk IIR PRN23/SVN60	0.9	−0.4	0.0	1.5	0.7	76.6	76.6
Blk IIR PRN28/SVN44	−0.2	−0.1	151.3	0.1	0.5	100.0	−51.4
Blk IIR-M PRN05/SVN50	−0.3	0.0	−1.7	−0.3	0.0	77.8	79.5
Blk IIR-M PRN07/SVN48	−0.1	0.0	0.1	0.0	0.5	82.2	82.2
Blk IIR-M PRN12/SVN58	1.0	−0.6	−9.4	1.0	−0.6	76.8	86.1
Blk IIR-M PRN15/SVN55	1.0	−0.6	−1.2	0.5	0.2	62.3	63.5
Blk IIR-M PRN17/SVN53	1.0	−0.6	−10.1	0.3	0.1	77.1	87.2
Blk IIR-M PRN29/SVN57	1.0	−0.6	−1.5	1.1	−0.5	79.2	80.7
Blk IIR-M PRN31/SVN52	−0.2	0.0	−5.8	−0.1	0.6	91.2	97.0
Blk IIF PRN01/SVN63	39.1	0.0	109.1	39.4	0.0	150.2	41.1
Blk IIF PRN03/SVN69	39.5	0.0	109.1	39.4	0.0	155.1	46.0
Blk IIF PRN06/SVN67	39.5	−0.1	109.2	39.4	0.0	146.7	37.5
Blk IIF PRN08/SVN72	39.6	0.0	108.6	39.4	0.0	150.1	41.6
Blk IIF PRN09/SVN68	39.6	−0.2	109.2	39.4	0.0	152.3	43.0
Blk IIF PRN10/SVN73	39.6	−0.1	108.3	39.4	0.0	151.5	43.2
Blk IIF PRN24/SVN65	39.2	0.2	109.3	39.4	0.0	140.7	31.4
Blk IIF PRN25/SVN62	39.2	0.2	109.3	39.4	0.0	151.7	42.4
Blk IIF PRN26/SVN71	39.5	−0.1	109.3	39.4	0.0	150.3	41.1
Blk IIF PRN27/SVN66	39.1	0.0	109.0	39.4	0.0	152.2	43.2
Blk IIF PRN30/SVN64	39.5	−0.1	109.0	39.4	0.0	152.2	43.2
Blk IIF PRN32/SVN70	39.7	0.0	108.4	39.4	0.0	153.5	45.0
Mean							43 ($\sigma = 47$)

* Offsets are represented in satellite body centered coordinates as defined by IGS body axes conventions (Montenbruck et al., 2015). NGA and 2SOPS values from (NGA 2018). ANTEX file downloaded February 24, 2020.

indication of a possible problem at a given epoch. To account for a possible time system difference, the navigation message clock offsets at a given time were shifted by a constant amount so that the mean of the clock offsets was the same for the navigation message and MGEX clocks. In all cases, a very small number of points were excluded due to the SISRE threshold; the case of BeiDou-2 MEO, IGSO, and GEO satellites had the largest number of points excluded, with 279 points (0.12% of available data points) excluded due to the SISRE threshold (most of which were GEO satellites). Aside from BeiDou-3, Table 1 shows that at least 94% of the maximum possible data points were used, with GPS and Galileo being over 99%. While only 75.3% of the maximum possible data points were used for BeiDou-3, this is mostly due to unavailable MGEX data for some satellites, for some portions of the 8-week span. Though the reasons for these gaps are not known, it is noted that BeiDou-3 was not officially operational during the time span used in this study.

The 7 similarity transformation parameters representing the systematic differences between each set of broadcast ephemerides and IGS14 are shown in Fig. 1. Following the convention used by the IERS, a positive rotation about an axis follows the 'left-hand rule'.

Once we form the set of ECEF satellite position vectors for a given constellation, and collect the corresponding set of position vectors from the MGEX files, we compare those two sets of vectors in a least-squares fit for the 7 similarity transformation parameters. We recognize that there is some prediction error in the broadcast messages and recognize that the MGEX positions, while regarded as superior in accuracy, are also not perfect. Since we have a very large number of points in our least squares fits (499,685 for example in the case of GPS as seen in Table 2), we expect that the predicted orbit errors (from broadcast messages) and post-fit orbit errors (from MGEX orbits) will not invalidate our choice of these 7 parameters but these orbit errors force us to acknowledge that our estimated parameters must be viewed as upper limits on the TRF levels of coincidence with IGS14. We do not attempt to isolate orbit prediction error from reference frame error. Note that a real-time user of GNSS also does not make this distinction. An unaugmented real-time GNSS user holds fixed the ECEF satellite position vectors in a real-time

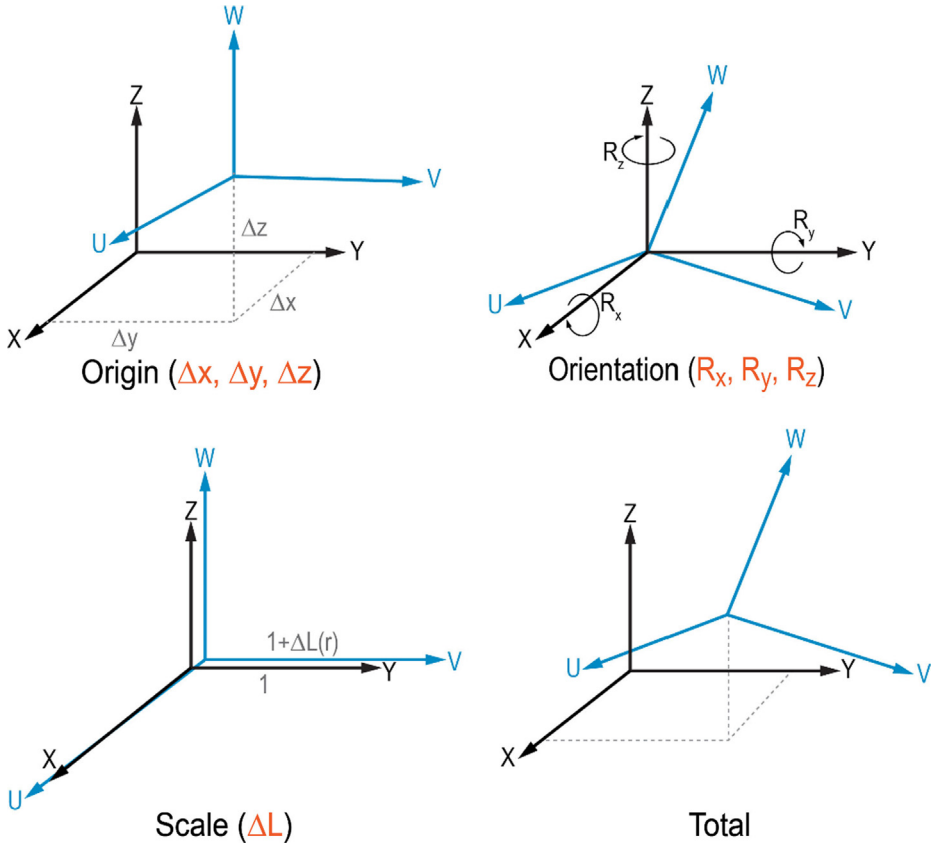

Fig. 1. The 7 similarity (Helmert) transformation parameters.

navigation solution. As mentioned above, these orbital realizations of a TRF represent the operational TRFs that billions of real-time GNSS users have access to.

Broadcast orbit errors and MGEX orbit errors have been quantified and documented in multiple publications. Montenbruck et al (2018) and Montenbruck et al (2017) are two comprehensive examples. Recent, traditional GNSS TRF comparisons based on fixed tracking stations on the Earth's crust can be found in Gusev (2019), Enderle (2018), and Liu et al. (2019). These customary ground-based geodetic TRF comparisons all report coincidence levels with the prevailing ITRF at the 1 cm level. Our results, based on orbital realization of a TRF are, as expected somewhat larger as seen in the results section below.

The 7 parameters that we show in Fig. 1 were estimated by finding the set of values that, when applied to the navigation message orbits, minimize the sum of the squares of the magnitude of the position differences between the navigation message and corresponding MGEX orbits. In an effort to simplify interpretation of the transformation parameters, we took an approximate but useful approach by converting the estimated rotation and scale parameters to linear units (cm) at the mean Earth radius and forming a Root-Sum-Square (RSS) of the 7 parameters for each GNSS.

$$RSS_7 = \sqrt{\Delta X^2 + \Delta Y^2 + \Delta Z^2 + \Delta L^2 + R_X^2 + R_Y^2 + R_Z^2} \qquad (1)$$

where the value of the mean Earth radius (6,371 km) yields conversion factors for 1 milli-arcsecond of rotation = 3.09 cm and 1 part per billion in scale = 0.64 cm. Since the vast majority of GNSS users are located on or near the Earth's surface, this approach appears reasonable. An alternate and perhaps more rigorous way to characterize the transformation parameters is to use the root-mean-square (RMS) average of the total position difference implied by the transformation at the surface of the Earth. This average is denoted by Λ and can be expressed as

$$\Lambda^2 = \frac{1}{4\pi}\int (\boldsymbol{r}' - \boldsymbol{r}) \cdot (\boldsymbol{r}' - \boldsymbol{r}) d\Omega, \qquad (2)$$

where $\boldsymbol{r}$ is the position vector of the point on the Earth's surface being considered, $\boldsymbol{r}'$ is the transformed position vector, and $d\Omega$ is the differential of the solid angle. The integral is taken over the entire surface of the Earth, which is assumed spherical with a radius of $r_e \approx 6{,}371$ km. Again, since the vast majority of GNSS users are located on or near the Earth's surface, this approach seems reasonable. Assuming that the overall transformation is sufficiently small, one can make the approximation

$$\boldsymbol{r}' - \boldsymbol{r} \approx \boldsymbol{a} + s\boldsymbol{r} + \theta_x \boldsymbol{r} \times \hat{x} + \theta_y \boldsymbol{r} \times \hat{y} + \theta_z \boldsymbol{r} \times \hat{z}, \qquad (3)$$

Table 3
Estimated transformation parameters using orbital realizations of a TRF.

GNSS	ΔX (cm)	ΔY (cm)	ΔZ (cm)	RX (mas)	RY (mas)	RZ (mas)	Scale (ppb)	RSS_7(cm)*	Λ(cm)*
GPS	0	0	5	−0.01	0.28	1.06	−0.27	6.0	5.7
GLONASS	0	0	10	0.21	0.00	1.76	−9.71	13.0	12.6
Galileo	2	0	2	−0.07	−0.19	−0.35	−1.81	3.3	3.2
BeiDou-2 (MEO)	11	3	42	−0.63	0.15	5.05	−18.97	47.8	47.0
(MEO,IGSO)	17	65	16	1.02	−2.42	7.53	−15.72	74.0	72.6
(MEO, IGSO, GEO)	39	59	44	−0.34	−2.72	3.75	−13.92	85.0	84.6
BeiDou-3	1	−1	3	0.10	−0.36	1.27	0.95	5.3	4.7

* RSS of 7 parameters has converted rotations and scale to linear units (cm) at the mean Earth radius.

Table 4
Standard deviations of the 8 weekly sets of transformation parameters and the associated RSS and Λ values.

GNSS	ΔX (cm)	ΔY (cm)	ΔZ (cm)	RX (mas)	RY (mas)	RZ (mas)	Scale (ppb)	RSS_7(cm)*	Λ(cm)*
GPS	1	1	2	0.57	0.87	1.17	0.11	5.4	4.6
GLONASS	2	2	6	0.26	0.52	2.78	0.57	11.0	9.8
Galileo	1	1	1	0.08	0.07	0.16	0.23	1.5	1.5
BeiDou-2 (MEO)	6	5	8	1.48	4.91	3.52	5.45	22.6	19.7
(MEO,IGSO)	9	10	7	1.65	3.16	3.01	2.25	21.3	19.6
(MEO, IGSO, GEO)	17	13	15	2.05	3.91	3.60	4.05	31.9	30.2
BeiDou-3	2	2	4	0.65	1.70	1.44	0.34	8.4	7.4

* RSS of 7 parameters has converted rotations and scale to linear units (cm) at the mean Earth radius.

where $\boldsymbol{a}$ is the translation vector and s is the relative scale factor. θ_x, θ_y, and θ_z are the x, y, and z rotation angles, respectively, in radians, while $\hat{x}$, $\hat{y}$, and $\hat{z}$ are unit vectors in the x, y, and z directions, respectively. Using this expression in the integral above yields

$$\Lambda^2 \approx \Delta X^2 + \Delta Y^2 + \Delta Z^2 + s^2 r_e^2 + \left(\theta_x^2 + \theta_y^2 + \theta_z^2\right)\frac{2r_e^2}{3}, \qquad (4)$$

where $\boldsymbol{a}$ has been broken into its components ΔX, ΔY, and ΔZ. Because all of the cross-terms vanish, Λ is just the RSS of the transformation parameters, where the scale and rotational parameters have been converted to distance by multiplying by r_e, in the case of the scale factor, and $\sqrt{2/3}r_e$, in the case of the rotational parameters. This implies conversion factors of 1 milli-arcsecond of rotation = 2.52 cm and 1 part per billion in scale = 0.64 cm.

The estimated 7 parameters from a single least squares fit for each GNSS over the entire 8-week span are shown in Table 3. Although not tabulated here, the parameters were also estimated for each individual week, and the standard deviations empirically computed from the population of 8 weekly sets of estimated parameters are shown in Table 4. The parameters estimated from a single fit using the full 8-week period were found to be nearly identical to the means of the values estimated from the 8 individual weeks.

We clearly observe that the origin offset in the Z direction (ΔZ) is the largest value in each case (each GNSS), except for BeiDou IGSO and GEO satellites. This general ΔZ result is seen fairly commonly in geodetic TRF comparisons and can be interpreted, in part, as a consequence of an uneven global distribution of tracking stations used by the providers across the northern and southern hemispheres as well as a consequence of orbital inclination. For example, errors in the orbit determination process are typically dominated by the along-track component and since a significant orbit plane inclination results in north–south or south-north directed errors, the Z component in a TRF realization becomes more difficult to establish. This interpretation is supported by the fact that among GPS, GLONASS, and Galileo, GLONASS has the largest orbit inclination and also has the largest ΔZ component shown in Table 3. Also note there are only 3 MEO BeiDou-2 satellites in this analysis, which significantly limits global coverage. The results for BeiDou-3 satellites (all MEO) benefit from a very good global distribution.

The empirical standard deviations shown in Table 4 are computed from the population of 8 individual weekly sets of estimates for the 7 parameters. Comparing Tables 3 and 4 shows that the standard deviations of the origin offsets and scale parameters are typically smaller than the estimated parameters themselves. The standard deviations on the orientation parameters are mixed; some are smaller and some are larger than the parameters themselves. The RSS and Λ values shown in Table 4 are computed from the standard deviations listed in the Table. We observe that the TRF realized by Galileo broadcast orbits clearly exhibits the best overall consistency with IGS14. Again, as stated above, we recognize that there is a level of orbit prediction error in the broadcast messages so we interpret the values shown on Table 3 as upper limits on these reference frame differences. The weekly repeatability repre-

sented in Table 4 also reveals (using the RSS_7 or Λ values) Galileo as the most stable TRF over the time period studied with GPS then BeiDou-3 then GLONASS in ranked order.

A comparison of our numerical results, shown in Tables 3 and 4, to an earlier published analysis of this nature included in Nicolini and Caporali (2018) indicates a significantly improved (smaller) set of estimated Helmert parameters and their corresponding dispersions in this study. The smaller Helmert parameters reported here indicate a better level of coincidence between a TRF realized via broadcast messages from an individual GNSS and the IGS14 TRF. The reasons for these improved levels of coincidence include: 1) far more data points used here over a longer time period (8 weeks vs 1 week of data) allowing more averaging of orbit error, 2) more rigorous handing of satellite antenna phase center offsets here, and 3) more complete Galileo and BeiDou constellations leading to improved global geometry for these GNSS. Future studies of this type are expected to reveal Helmert parameters equal to or smaller than those shown in Tables 3 and 4. GNSS operators are likely to continue the trend of implementing incremental improvements in their real-time estimation and broadcast message distribution processes.

Because our RSS_7 quantity, and the alternate quantity Λ, described above have to date, not been used in published studies as a metric for TRF comparisons, we tested and demonstrated its usefulness by applying the concept to the series of Helmert transformations published by the IERS which characterize the systematic differences between ITRF2014 and previous ITRF realizations. The values used in this analysis were obtained from: http://itrf.ign.fr/doc_ITRF/Transfo-ITRF2014_ITRFs.txt, downloaded 29 Oct 2019. A histogram of the RSS_7 values for the series of ITRFs is shown in Fig. 2. A plot using the Λ parameter would appear very similar. This figure supports the widespread understanding that the ITRFs have been systematically improved since 1988, therefore demonstrating the usefulness of this single metric as a way to characterize TRF coincidence. The outlier seen in the figure for ITRF93 is dominated by the rotation angles that established ITRF93. For this frame, a constraint was used which ensured frame orientation consistency with the IERS series of Earth Orientation Parameters (EOP) (Boucher et al., 1994). That approach was only used once in the history of ITRF realizations. For ITRF94, the orientation was constrained to match the orientation of ITRF92 (not ITRF93) at epoch 1988.0, thereby abandoning the EOP constraint approach used to orient ITRF93 (Boucher et al., 1996). All subsequent ITRF realizations, as well as those prior to ITRF93, were constrained to the orientation of its predecessor at a specific epoch. The first ITRF, ITRF88, was constrained to match the orientation of the Bureau International de l'Heure (BIH) series of TRFs, the first of which was BTS84 at epoch 1984.0 (Boucher and Altamimi, 1989).

4. The GNSS realizations of prime meridians

If we focus on one of the 7 Helmert parameters shown in Table 3, namely, the rotation around the Cartesian Z axis, we can interpret these values as each GNSS' realization of the X-Z plane or in other words, the location of each GNSS' realization of a zero meridian, with respect the realization of the IGS14 zero meridian. These relationships, for the 56-day data period studied, are shown in Fig. 3. The estimated standard deviation is plotted along with the rotation parameter. We observe that Galileo's realization of a

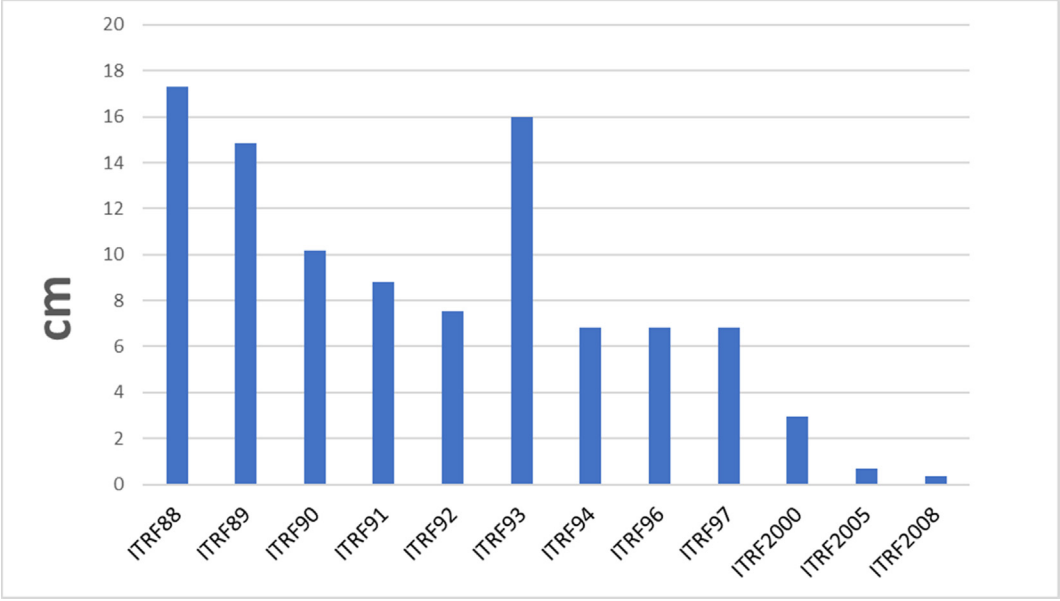

Fig. 2. Root Sum Square of 7 Transformation parameters from ITRF2014 to previous ITRFs. Rotation and scale parameters have been converted to linear units at the mean Earth radius. Data source is http://itrf.ign.fr/doc_ITRF/Transfo-ITRF2014_ITRFs.txt, downloaded 29 Oct 2019.

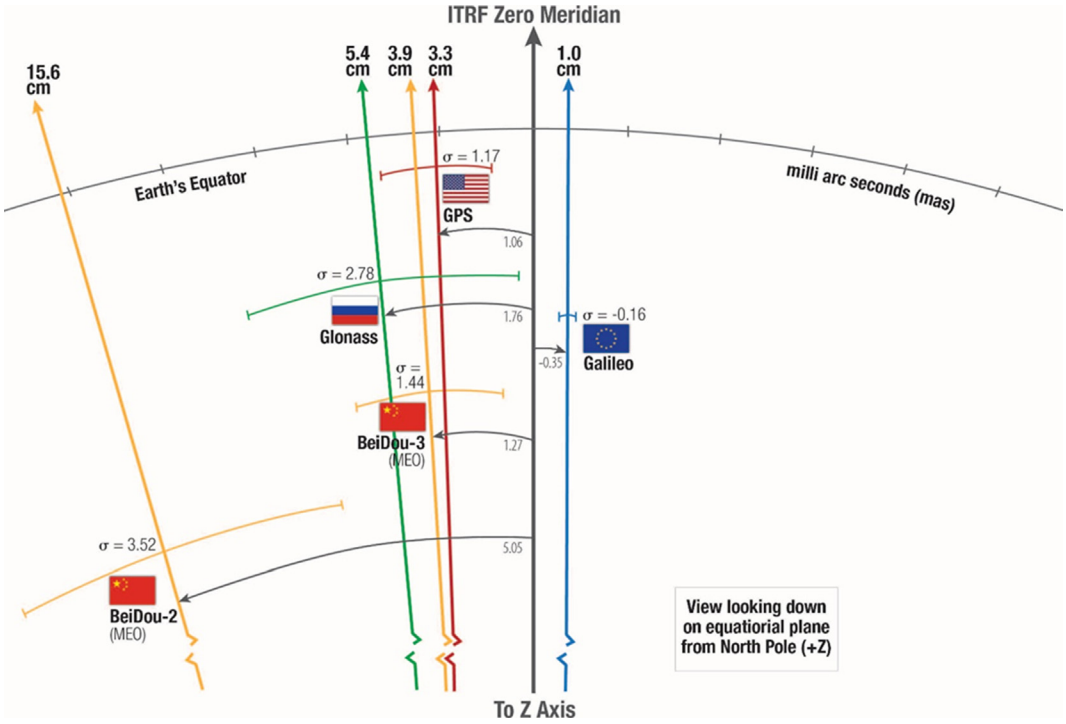

Fig. 3. GNSS realization of a prime meridian with respect to the IGS14 zero meridian during the period 21 July-14 September 2019.

zero meridian exhibits the best agreement with the ITRF zero meridian and also exhibits the smallest standard deviation.

5. Summary and conclusions

Our analysis begins by accepting the notion that IGS14 is the best available realization of a Terrestrial Reference Frame using GNSS. We demonstrate a systematic improvement in ITRFs by using a simplified representation (RSS_7) of Helmert parameters expressed at the mean Earth radius. Among the four GNSS studied, we observe that the TRF realized by Galileo broadcast orbits clearly exhibits the best overall consistency with IGS14. Galileo also exhibits the best level of stability over the 8 week period studied. Because the broadcast navigation messages contain predictions of satellite ephemerides, these messages inherit random and systematic errors from a number of sources. As such, the estimated 7 parameter transformations reported here should be interpreted as upper limits on the coincidence level of each GNSS TRF with respect to IGS14. Predictions of along-track orbit positions, for example, are notoriously more difficult to obtain and therefore the comparisons performed here are likely to include these along-track errors at some level.

The simplified RSS_7 quantities represented by Eq. (1), as well as an alternate method based on the total transformation vector, indicate that the TRF coincidence levels differ from IGS14 at a level no greater than 4 cm for Galileo, 6 cm for GPS and BeiDou-3, 13 cm for GLONASS, and 48 cm for a limited set of BeiDou-2 Medium Earth Orbit (MEO) vehicles. The weak geometry represented by BeiDou-2 ISGO and GEO vehicles creates a limitation in this analysis in part because these vehicles are not distributed globally.

These numerical results represent orbital realizations for Terrestrial Reference Frames achieved and accessible by real-time GNSS users. Integrators and developers of Multi-GNSS processes may find these results helpful as error budgets for those processes are developed.

Declaration of Competing Interest

The authors declare that they have no known competing financial interests or personal relationships that could have appeared to influence the work reported in this paper.

Acknowledgements

We gratefully acknowledge the many individual contributors and institutions that have made the International GNSS Service (IGS) and the MGEX activity the valuable resources that they have become. Personnel who maintain NASA's CDDIS are notable contributors. The tremendous discipline and rigor demonstrated by members of both the IGS and the IERS are gratefully recognized. We also wish to thank the reviewers of this manuscript for very constructive suggestions and timely response.

References

Altamimi, Z., Rebischung, P., Metivier, L., Collilieux X., ITRF2014: A new release of the International Terrestrial Reference Frame modeling nonlinear station motions. J. Geophys. Res.-Solid Earth, Vol. 12, Issue: 8, 6109-6131.

Altamimi, Z., Rebischung, P., Métivier, L., Collilieux, X., 2017. Analysis and results of ITRF2014. (IERS Technical Note 38) Frankfurt am Main: Verlag des Bundesamts für Kartographie und Geodäsie, 2017. 76 pp., ISBN 978-3-86482-088-5.

Bar-Sever, Y.E., Bertiger, W.I., Davis, E.A.S., Anselmi, J.A., 1996. Fixing the GPS Bad Attitude: Modeling GPS Satellite Yaw During Eclipse Seasons. Navigation 43 (1), 25–40.

Boucher, C., Altamimi, Z., 1989. The Initial IERS Terrestrial Reference Frame, IERS Technical Note 1. Central Bureau of IERS, Observatoire de Paris.

Boucher, C., Altamimi, Z., Duhem, L., 1994. Results and Analysis of the ITRF93, IERS Technical Note 18. Central Bureau of IERS, Observatoire de Paris.

Boucher, C., Altamimi, Z., Feissel, M., Sillard, P., 1996. Results and Analysis of the ITRF94, IERS Technical Note 20. Central Bureau of IERS, Observatoire de Paris.

Boucher, C., Altamimi, Z., 2001. ITRS, PZ-90 and WGS 84: current realizations and the related transformation parameters. J. Geodesy, Vol. 7, Issue 11, pp. 613-619.

CNSO, 2016. (China Satellite Navigation Office), BeiDou Navigation Satellite System Signal in Space Interface Control Document Open Service. Signal V2, 1.

Dick, W., Thaller, D., (Eds.) IERS Annual Report 2018. International Earth Rotation and Reference Systems Service, Central Bureau. Frankfurt am Main: Verlag des Bundesamts für Kartographie und Geodäsie, 2020. 207 p., ISBN 978-3-86482-136-3.

Dilssner, F., 2010. GPS IIF-1 Satellite Antenna Phase Center and Attitude Modeling, Inside GNSS, September 2010, 59–64.

Dilssner, F., Springer, T., Gienger, G., Dow, J., 2010. The GLONASS-M Satellite Yaw-Attitude Model. Adv. Space Res. 47 (1), 160–171.

Dow, J.M., Neilan, R.E., Rizos, C., 2009. The International GNSS Service in a changing landscape of Global Navigation Satellite Systems. J. Geodesy 83, 191–198. https://doi.org/10.1007/s00190-008-0300-3.

EU, 2016. European GNSS (Galileo) Open Service Signal in Space Interface Control Document, OS SIS ICD, Iss. 1.3, Dec. 2016.

Griffiths, J., 2019. Combined orbits and clocks from IGS second reprocessing. J. Geodesy 93, 177–195. https://doi.org/10.1007/s00190-018-1149-8.

Johnston, G., Riddell, A., Hausler, G., 2017. The International GNSS Service. In: Teunissen, P., Montenbruck, O. (Eds.) Springer Handbook of Global Navigation Satellite Systems, DOI: 10.1007/978-3-319-42928-1_33.

Lewandowski, W., Arias, E.F., E.F., GNSS Times and UTC, Metrologia, 2011. 48 S219, doi:10.1088/0026-1394/48/4/S14.

Malys, S., Slater, J., 1994. Maintenance and Enhancement of the World Geodetic System 1984. In: Proceedings ION-94, Salt Lake City, Utah.

Montenbruck, O., Steigenberger, P., 2013. The BeiDou Navigation Message. IGNSS Symposium.

Montenbruck, O., Schmid, R., Mercier, F., Steigenberger, P., Noll, C., Fatkulin, R., Kogure, S., Ganeshan, A.S., 2015. GNSS satellite geometry and attitude models. Adv. Space Res. 56 (6), 1015–1029. https://doi.org/10.1016/j.asr.2015.06.019.

Montenbruck, O., Steigenberger, P., Prange, L., Deng, Z., Zhao, Q., Perosanz, F., Romero, I., Noll, C., Stürze, A., Weber, G., Schmid, R., MacLeod, K., Schaer, S., 2017. The Multi-GNSS Experiment (MGEX) of the International GNSS Service (IGS) – Achievements, Prospects and Challenges. Adv. Space Res. 59 (7), 1671–1697. https://doi.org/10.1016/j.asr.2017.01.011.

Montenbruck, O., Steigenberger, P., Hauschild, A., 2018. Multi-GNSS signal-in-space range error assessment - Methodology and results. Adv. Space Res. 61 (12), 3020–3038. https://doi.org/10.1016/j.asr.2018.03.041.

NAVSTAR GPS Space Segment/Navigation User Segment Interfaces, ICD-GPS-200, May, 2020.

Noll, C.E., 2010. The crustal dynamics data information system: A resource to support scientific analysis using space geodesy. Adv. Space Res. 45 (12), 1421–1440. https://doi.org/10.1016/j.asr.2010.01.018.

Pearlman, M.R., Degnan, J.J., Bosworth, J.M., 2002. The International Laser Ranging Service. Adv. Space Res. 30 (2), 135–143.

Petit, G., Delporte, J., December 2019. WG D Task Force on Time references Update of actions since ICG-13, Fourteenth Meeting of the International Committee on GNSS, ICG-14, 8–13. Bangalore, India.

Rebischung, P., Altamimi, Z., Ray, J., Garayt, B., 2016a. The IGS contribution to ITRF2014. J. Geodesy 90, 611–630. https://doi.org/10.1007/s00190-016-0897-6.

RISDE (Russian Institute of Space Device Engineering), ICD L1, L2 GLONASS, Moscow, 2008.

Schmid, R., Dach, R., Collilieux, X., Jäggi, A., Schmitz, M., Dilssner, F., 2016. Absolute IGS antenna phase center model igs08.atx: status and potential improvements. J. Geod. 90 (4), 343–364.

Schuh, H., Behrend, D., 2012. VLBI: A fascinating technique for geodesy and astrometry. J. Geodyn. 61, 68–80. https://doi.org/10.1016/j.jog.2012.07.007.

Slater, J.A., Noll, C.E., Gowey, K.T. (Eds.), International GLONASS Experiment, IGEX-98 Workshop. In: Proceedings, Nashville, Tenn., Sept. 13-14, 1999 (NASA/JPL Pub. 00-0006, Apr. 2000).

Willis, P., Beutler, G., Gurtner, W., Hein, G., Neilan, R., Noll, C., Slater, J., 1999. IGEX: International GLONASS experiment — Scientific objectives and preparation. Adv. Space Res. 23 (4), 659–663.

Willis, P. et al., 2010. The International DORIS Service: Toward maturity. Adv. Space Res. 45 (12), 1408–1420. https://doi.org/10.1016/j.asr.2009.11.018.

Web References

CNSO (China Satellite Navigation Office), BeiDou ANTEX File, [Online]. Available: http://www.beidou.gov.cn/yw/gfgg/201912/W020191230559858078729.atx. [Accessed 28 February 2020].

Dilssner, F., A Note on the Attitude Model of BeiDou IGSO-6, 2017. [Online]. Available: http://navigation-office.esa.int/attachments_24576369_1_BeiDou_IGSO-6_Yaw_Modeling.pdf. [Accessed 21 February 2020].

Dilssner, F., Laufer, G., Springer, T., Schonemann, E., Enderle, W., 2018. The BeiDou Attitude Model for Continuous Yawing MEO and IGSO Spacecraft, 2018. [Online]. Available: http://navigation-office.esa.int/attachments_29393052_1_EGU2018_Dilssner_Final.pdf. [Accessed 21 February 2020].

Enderle, W., 2018. Galileo Terrestrial Reference Frame (GTRF)- Status, Fourteenth Meeting of the International Committee on GNSS, ICG-13, 04-09 November 2018, Xi'an, China, UNOOSA https://www.unoosa.org/documents/pdf/icg/2018/icg13/wgd/wgd_06.pdf.

EU, European Global Navigation Satellite Systems Agency, Galileo Satellite Metadata, [Online]. Available: https://www.gsc-europa.eu/support-to-developers/galileo-satellite-metadata. [Accessed 28 August 2020].

Gusev, I., 2019. GLONASS Reference Frame Evolution, Fourteenth Meeting of the International Committee on GNSS, ICG-14, 8-13, Bangalore, India, December 2019, UNOOSA https://www.unoosa.org/documents/pdf/icg/2019/icg14/WGD/icg14_wgd_02.pdf.

IGS ANTEX File (Week 2091) [Online]. Available: ftp://www.igs.org/pub/station/general/pcv_archive/igs14_2091.atx [Accessed 24 February 2020].

IGS Mail 7921, IGS Mail Archive, Available at: https://lists.igs.org/mailman/listinfo/igsmail.

Liu, L., Xu, J., Zhou, S., Wu, F., 2019. Update on the BeiDou Coordinate System(BDCS). In: Fourteenth Meeting of the International Committee on GNSS, ICG-14, 8-13, Bangalore, India, December 2019,

UNOOSA https://www.unoosa.org/documents/pdf/icg/2019/icg14/WGD/icg14_wgd_01.pdf.

Malys, S., Wong, R., True S., 2016. The WGS 84 Terrestrial Reference Frame in 2016. In: Eleventh Meeting of the International Committee on GNSS, ICG-11, 6-11 November 2016, Sochi, Russia, UNOOSA https://www.unoosa.org/pdf/icg/2016/icg11/wgd/02wgd.pdf.

NGA, 2018. NGA GNSS Division Precise Ephemeris Parameters, Effective Date Oct 31, 2018. National Geospatial-Intelligence Agency. ftp://ftp.nga.mil/pub2/gandg/website/gnss/data/prod_docs/NGA%20GNSS%20Precise%20Ephemeris%20Parameters.pdf.

Rebischung, P., Schmid, R., Herring, T., 2016. Upcoming switch to IGS14/igs14.atx. IGSMAIL-7399. https://lists.igs.org/pipermail/igs-mail/2016/001233.html.